Neuron, Vol. 23, 449–459, July, 1999, Copyright ©1999 by Cell Press

# Identification of Neural Circuits by Imaging Coherent Electrical Activity with FRET-Based Dyes

Neurotechnique

**Timothy W. Cacciatore,[1] Peter D. Brodfuehrer,[7] Jesus E. Gonzalez,[8] Tao Jiang,[8] Stephen R. Adams,[4] Roger Y. Tsien,[1,3,4,6] William B. Kristan, Jr.,[1,2] and David Kleinfeld[1,5,9]**

[1]Group in Neurosciences
[2]Department of Biology
[3]Department of Chemistry and Biochemistry
[4]Department of Pharmacology
[5]Department of Physics
[6]Howard Hughes Medical Institute
University of California, San Diego
La Jolla, California 92093
[7]Department of Biology
Bryn Mawr College
Bryn Mawr, Pennsylvania 19010
[8]Aurora Biosciences
San Diego, California 92121

## Summary

**We show that neurons that underlie rhythmic patterns of electrical output may be identified by optical imaging and frequency-domain analysis. Our contrast agent is a two-component dye system in which changes in membrane potential modulate the relative emission between a pair of fluorophores. We demonstrate our methods with the circuit responsible for fictive swimming in the isolated leech nerve cord. The output of a motor neuron provides a reference signal for the phase-sensitive detection of changes in fluorescence from individual neurons in a ganglion. We identify known and possibly novel neurons that participate in the swim rhythm and determine their phases within a cycle. A variant of this approach is used to identify the postsynaptic followers of intracellularly stimulated neurons.**

## Introduction

Rhythmic motor behaviors, such as locomotion, are usually produced by neuronal circuits that function in the absence of peripheral feedback (Delcomyn, 1980). These circuits, denoted central pattern generators (CPGs), serve as model systems for studying the emergence of stable neuronal activity as a function of the biophysical properties of the constituent neurons and the architecture of the underlying circuit (Marder and Calabrese, 1996). However, a correspondence between measurements of the output patterns from such circuits and the predictions from models of neural networks have been achieved only for a limited number of CPGs (Satterlie, 1985; Kleinfeld and Sompolinsky, 1988; Getting, 1989; Grillner et al., 1991; Calabrese et al., 1995). A major difficulty in determining the architecture of circuits that produce rhythmic outputs is simply to identify which neurons are active in a given rhythm. The traditional strategy is to record from pairs or n-tuples of cells with intracellular electrodes (Selverston and Moulins, 1987), which unfortunately becomes unwieldy when many tens or hundreds of neurons are present in a ganglion.

Cohen, Salzberg, and their colleagues (Salzberg et al., 1977; Zecevic et al., 1989; Obaid et al., 1999) introduced the use of optical imaging of neurons stained with molecular indicators of membrane potential as a means of surmounting the problem of simultaneously recording the output from most of the neurons in a ganglion. This information could, in principle, be used to identify those neurons that are active during a rhythmic behavior and, further, to guide the placement of electrodes in the active cells for detailed analysis. In practice, the successful pairing of anatomically identified neurons with the measured neuronal outputs was not carried out. Further, previous studies focused exclusively on the spiking output from neurons and did not report subthreshold activity.

Here, we readdress the use of optical imaging as a means of surveying the electrical output of neurons that participate in the generation of rhythmic output and of detecting connections among these neurons. We introduce two technical advances that allow us to overcome some of the previous limitations with this approach. First, we use a two-component dye system in which changes in transmembrane potential are detected via fluorescent resonant energy transfer (FRET) between a membrane-bound fluorophore and a charged, membrane-mobile fluorophore (Gonzalez and Tsien, 1995, 1997). The sensitivity of this system is governed by electrodiffusion and, in practice, is much higher than that achieved with traditional voltage-sensitive dyes, in which a single chromophore interacts directly with the transmembrane electric field (Loew et al., 1979). Second, we employ frequency-domain techniques to detect and quantitate rhythmic optical signals in terms of their spectral coherence with respect to an electrical reference as a means of maximizing our sensitivity with low signal-to-noise ratios. Further, we average over independent estimates of the coherence (Thomson, 1982) as a means of evaluating the statistical significance of our measurements.

We applied the above techniques to the swim CPG of the leech. Initial studies identified a small set of interneurons in each ganglion that act as a triphasic oscillator (Friesen et al., 1976; Stent et al., 1978), which drives motor neuron output. Subsequent studies suggested that the original circuit model was incorrect and that additional interneurons are apparently needed to explain the generation of the swimming rhythm (Weeks and Kristan, 1978; Brodfuehrer et al., 1995). Thus, the introduction of new methodologies to study this circuit presents an opportunity to corroborate our results against published reports as well as to search for additional neurons that contribute to the rhythm.

## Results

### Optimization of the Dye System

We used a combination of two fluorophores (Figure 1A). An impermeant amphiphilic coumarin conjugate binds

[9]To whom correspondence should be addressed (e-mail: dk@physics.ucsd.edu).

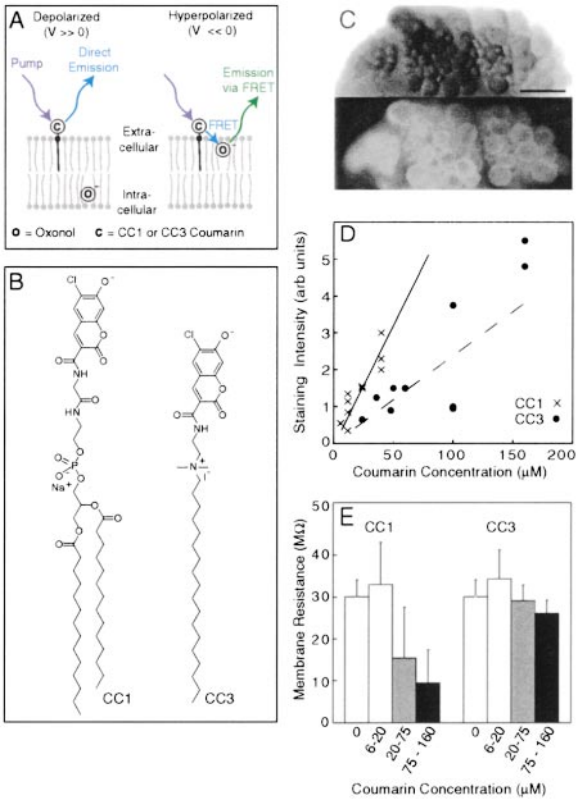


Figure 1. Incorporation of FRET-Based Dyes into Neuronal Membranes

(A) Cartoon of the mechanism for voltage sensing via FRET frame coumarin to a mobile oxonol molecule in the membrane.

(B) Structure and charge, at physiological pH, of N-(6-chloro-7-hydroxycoumarin-3-carboxamidoacetyl)-dimyristoylphosphatidylethanolamine (CC1) and CC3.

(C) Full-resolution digital images of the dorsal side of a desheathed, isolated midbody ganglion. Shown on the top is the image under dark-field illumination, contrast reversed for clarity, and shown on the bottom is the fluorescent image after staining the ganglion in 100 μM of CC3 coumarin. An unstained ganglion had 100-fold less emission. Scale bar, 100 μm.

(D) The relative emission from neurons in ganglia stained with the CC1 versus CC3 coumarin as a function of dye concentration ($n = 7$ preparations); the data were taken under identical levels of incident illumination. The straight lines indicate a least-squares fit.

(E) The membrane resistance of identified neurons (N cells) stained with either CC1 or CC3 coumarin as a function of dye concentration. Recordings were made with a two-electrode voltage clamp, using 10 mV steps from a holding potential of −50 mV, at least 45 min after staining.

to the outer leaflet of the cell membrane and is directly excited by the incident illumination. A negatively charged oxonol molecule shuttles across the hydrophobic core of the membrane and is distributed between the outer and inner leaflets of the membrane according to the transmembrane potential (Gonzalez and Tsien, 1997). The absorption spectrum of the coumarin had minimal overlap with that of the oxonol, such that there was negligible direct excitation of the oxonol. On the other hand, the emission spectrum of the coumarin had substantial overlap with the absorption spectrum of the oxonol, such that the coumarin could efficiently transfer energy to nearby oxonols on the outer leaflet via FRET (Forster, 1948). Changes in membrane potential are inferred from changes in the extent of emission from the directly excited coumarin and/or the resonantly excited oxonol.

We screened two different coumarin molecules, a previously described phosphatidylethanolamine derivative (CC1) (Gonzalez and Tsien, 1997) and a newly synthesized compound, N−(2−[octadecyldimethylammonio] ethyl)-6-chloro-7-hydroxycoumarin-3-carboxamide (CC3) (Figure 1B) (see Experimental Procedures). Application of either molecule to desheathed ganglia resulted in strong staining of essentially all somata (cf. dark-field and fluorescent images; Figure 1C) and weak staining of the neuropil. Although neurons were stained more strongly with the CC1 coumarin at equal concentrations of the dyes (Figure 1D), the CC1 coumarin caused appreciable degradation of cellular structure and decreased resistance of cell membranes for concentrations above 20 μM (Figure 1E). In contrast, the CC3 coumarin did not significantly affect membrane resistance at concentrations up to 160 μM, which corresponds to the brightness of staining achieved with concentrations of CC1 of ~50 μM. All subsequent measurements were performed with ganglia stained with 100 μM solutions of CC3.

Oxonols may be synthesized with a range of hydrophobicities. Increasing hydrophobicity makes the dye more difficult to load into cell membranes but speeds the equilibration of the dye across the membrane in response to changes in transmembrane potential. Since the changes in potential associated with the swim rhythm are slow (cycle frequency of $\upsilon \approx 1$ Hz), we used a relatively hydrophilic oxonol (see Experimental Procedures) to ensure ready access of the dye to neuronal membranes. The oxonol did not significantly affect membrane resistance for concentrations of up to 12 μM (data not shown). Unless noted, all measurements were performed with ganglia stained in 8 μM solutions.

### Nature of the Dye Signals

We considered first the response in single neurons that were driven by the intracellular injection of a sinusoidal current (Figure 2A). The normalized change in emission from the oxonol, denoted ΔF/F, consisted of an oscillatory component and a slow drift caused by bleaching of the coumarin (oxonol [raw] trace; Figure 2A). The slow drift was subtracted (see Experimental Procedures), and the resultant oscillatory signal was seen to covary with the applied voltage (oxonol trace; Figure 2A). The emission from the oxonol decreased with an increase in transmembrane potential, consistent with a decrease in FRET, when the distribution of the negatively charged oxonols was shifted away from the coumarin molecules in the outer leaflet of the membrane. Further, the emission from the coumarin was precisely out of phase with that from the oxonol (Figure 2B).

We examined the sensitivity of the change in emission from the oxonol as a function of transmembrane potential. Individual neurons were driven by applying square waves, 5–10 mV in amplitude and with a frequency of 1 Hz, under voltage clamp. We measured the fractional change in fluorescence at the drive frequency from different transmembrane holding potentials. The sensitivity

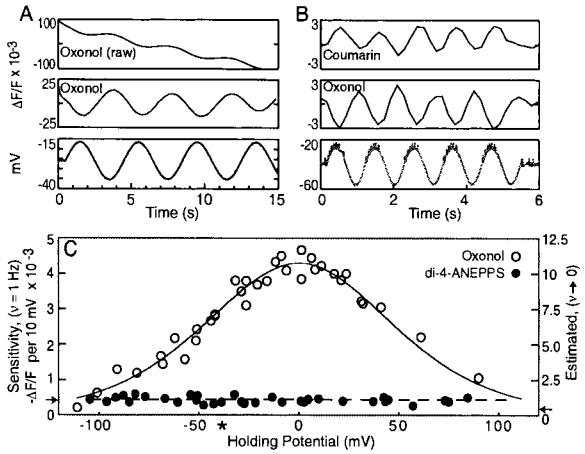


Figure 2. Characterization of the Optical Response

Ganglia were stained with CC3 coumarin and oxonol.

(A) The fractional change in emission from oxonol in response to a single trial of four cycles of 0.25 Hz sinusoidal stimulation. Data were obtained from Retzius cells under two-electrode voltage clamp. The top trace shows the normalized (ΔF/F) but otherwise unprocessed recording. The middle trace is the same recording after a slow drift caused by bleaching has been subtracted. The bottom trace is the measured membrane potential.

(B) The fractional change in the emission from coumarin and oxonol measured in response to intracellular stimulation with a sinusoidal current (1 nA amplitude, 1 Hz) of an anterior pagoda (AP) cell under two-electrode current clamp. The two optical signals were obtained in sequential trials from the same cell. The voltage traces for the two trials are superimposed.

(C) The sensitivity of emission from oxonol and from di-4-ANEPPS as a function of membrane potential. We used AP neurons under a two-electrode voltage clamp and rhythmically drove the neurons at various holding potentials with 1 Hz square waves with a 10 mV amplitude. Data with holding potentials above 0 mV were obtained by using leech Ringer solution with $Na^+$ replaced by N-methyl-D-glucamine, and intracellular electrodes filled with 10 mM tetraethylammonium to block action potentials. The asterisk indicates typical resting potentials of leech neurons. The curve is a fit of Equation 2 with $\beta = 0.82$ and $A = 0.027$. The right-hand axis is the extrapolated value of $\Delta F/F$ as the drive frequency goes to zero, using $\Delta F(\upsilon \rightarrow 0)/F = 2.5\ \Delta F(\upsilon = 1\ Hz)/F$ from the data of Figure 3B; the right-hand arrow points to the rescaled value of $-\Delta F/F$ for di-4-ANEPPS.

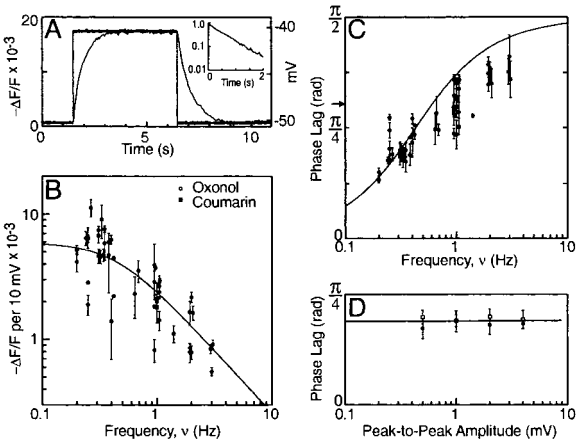


Figure 3. Temporal Characterization of the FRET Response

(A) The change in normalized oxonol emission, $-\Delta F/F$, in a Retzius cell in response to a 10 mV voltage step under two-electrode voltage clamp. The data is from a single trial.

(Inset) The initial 2 s of the response $\Delta F/F$, normalized to lie in the interval (0,1], plotted on a log scale. The observed time constant is proportional to the slope of this line and is $\tau = 0.45$ s.

(B) The magnitude of the normalized change in emission from oxonol as a function of the frequency of oscillations in the membrane potential. The data represent a survey of seven cell types (Retzius, N, P, Lydig, AP, Cell 1, and Cell 3), and the neurons were driven with a two-electrode voltage clamp using sinusoids that were 5 mV in amplitude from a holding potential of $-40$ mV. Each data point represents two to six trials (10–50 cycles) in one cell. The data are plotted as mean ± SD. The line is the equation for the magnitude of the frequency representation of a single exponential response, i.e., $\Delta F(\nu)/F = [\Delta F(\nu \rightarrow 0)/F]/\sqrt{1 + (2\pi\nu\tau)^2}$, with $\tau = 0.36$ s and $-\Delta F(\nu \rightarrow 0)/F = 7.2 \times 10^{-3}$ for a 10 mV change.

(C) Phase of the coherence between the optical signal and the electrical reference as a function of frequency using the same data as in (B). The line is the equation for the phase of the frequency representation of a single exponential response, i.e., $\phi_{opt\text{-}elec} = \tan^{-1}(2\pi\nu\tau)$, with $\tau = 0.36$ s. The arrow indicates the averaged measured shift at 1 Hz, i.e., $\phi_{opt\text{-}elec} = 0.30\ \pi \pm 0.04\ \pi$ radians.

(D) The phase of the coherence between the oxonol signal and the intracellular potential as a function of the voltage amplitude of the rhythmic drive signal; neurons were driven at $\upsilon = 0.3$ Hz under voltage clamp. Closed and open circles correspond to data obtained with two different neurons.

to changes in membrane potential had a peak at a holding potential of 0 mV and declined to near zero at potentials of ±100 mV (Figure 2C). The data were well fit by the Boltzman statistics for a two-state system under the influence of a potential (see Experimental Procedures). The adjustable parameters are a scale factor, denoted $\beta$, that corresponds to the fraction of the potential drop across the hydrophobic core of the membrane, which is sensed by the oxonol, and to an overall amplitude (Equation 2). We found that $\beta = 0.82 \pm 0.02$ (mean ± SEM), consistent with past estimates (Tsien, 1976). For the conditions of these measurements (40× objective, $\upsilon = 1$ Hz), the maximum sensitivity was $|\Delta F/F| = 4.3 \times 10^{-3}$/10 mV (4.3%/100 mV). Additional measurements at a select number of points indicated that the sensitivity curve was unchanged for oxonol concentrations of 4 μM and 12 μM (data not shown). Finally, the coumarin emission had a similar voltage dependence, with a maximum sensitivity of $|\Delta F/F| = 2.1 \times 10^{-3}$/10 mV (data not shown), reflecting the smaller normalized signal recorded from the coumarin versus the oxonol. In all subsequent measurements, we recorded only the larger oxonol emission.

It is useful to compare the sensitivity achieved with the two-component FRET dye system with that obtained with neurons stained with a "standard" voltage-sensitive dye. We selected 1-(3-sulfonatopropyl)-4-(β-[2-(di-N-butylamino)-6-naphthyl]vinyl) pyridinium betaine (di-4-ANEPPS) (Fluhler et al., 1985), which yields particularly strong signals in a variety of intact preparations (Delaney al., 1994; Youngentob et al., 1995; Canepari et al., 1996; Yuste et al., 1997), and measured the sensitivity of the change in emission with excitation and emission filters optimized for di-4-ANEPPS (see Experimental Procedures). The observed change was $|\Delta F/F| = 0.5 \times 10^{-3}$/10 mV (Figure 2C), consistent with that in a previous study on intact leech ganglia (Canepari et al., 1996), and the sensitivity was independent of holding potential, as

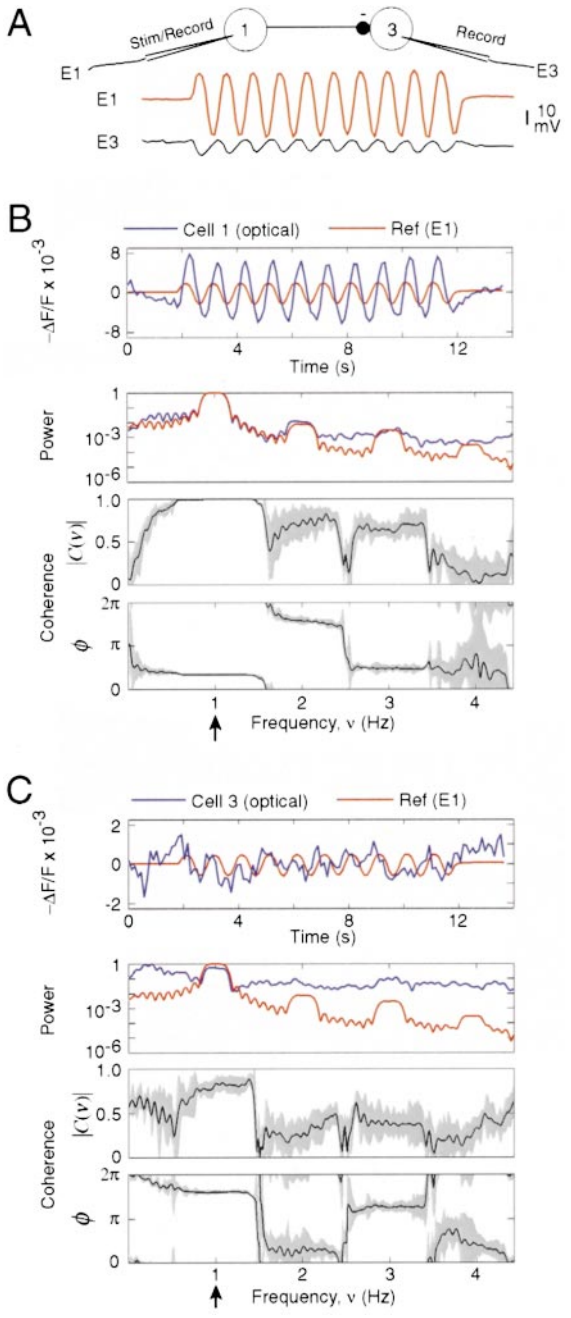


Figure 4. Optical Responses of Dorsal Neurons to Sinusoidal Current Injected into Cell 1 (2 nA, 1 Hz)

All data are from a single 14 s trial. Traces in red always refer to the intracellular recording from Cell 1, while blue traces refer to optical recordings from Cell 1 or 3 as indicated.

(A) Records of the simultaneous intracellular measurements from Cell 1 (E1) and Cell 3 (E3).

(B) Superimposed optical and electrical signals for Cell 1 (top), the spectral power for both signals (middle), and the magnitude and phase of their coherence (bottom). The gray envelope in the coherence traces delimits the standard deviation. Note that the spectral power estimated for the optical signal has a peak at the frequency used to drive Cell 1. The phase of the optical signal relative to the underlying transmembrane potential is observed to lag by 0.35 $\pi$ radians, consistent with that found for other cell types (Figure 3C).

(C) Superimposed optical signals for Cell 1 and the electrical reference signal from Cell 3. All conditions are the same as for (B), except that we compare the optical response of Cell 3 to the reference (E1). Note that the phase of the coherence at 1 Hz for Cell 1 is significantly different from that for Cell 3.

expected (Fluhler et al., 1985; Fromherz and Lambacher, 1991). Thus, the FRET dye system is many-fold more sensitive than di-4-ANEPPS.

The increased sensitivity of the FRET system comes with two penalties. The sensitivity of the voltage dependence, $|\Delta F/F|/\Delta V$, is a bell-shaped curve (Equation 2) whose value changes over voltage excursions on the scale of $2kT/\beta e \approx 60$ mV (Figure 2C), where k is Boltzman's constant, T is the absolute temperature, and e is the electronic charge. Only the responses at unphysiologically hyperpolarized or depolarized potentials are greatly diminished. The other disadvantage is a relatively slow response time, caused by the limited hydrophobicity of the oxonol chosen for the present study. The equilibration of the oxonol between the outer and inner leaflets of the membrane obeys single exponential kinetics (Gonzalez and Tsien, 1995), whose time constant is denoted $\tau$. We determined $\tau$ in leech neurons by two methods, described below.

We first measured the value of $\tau$ directly from the time dependence of the change in emission from oxonol in response to a step in the holding potential of neurons. For potentials in the range of $-60$ to $-40$ mV, which approximate those in active swim neurons (Ort et al., 1974), and voltage steps between 5 and 20 mV, we observed that the response of the dye was well described by a single exponential with a time constant of $\tau = 0.44 \pm 0.06$ s (mean $\pm$ SEM, n = 6) (Figure 3A).

The value of the time constant limits our ability to resolve the periodic components of the optical signals. For voltage changes that are small on the scale of thermal potential (60 mV), the amplitude of the optical signal and the associated phase shift between the optical signal and the underlying change in transmembrane potential are expected to follow the frequency representation of an exponential decay. Nonetheless, our assignment of relative phases to the activity of different neurons will not be affected so long as the phase shifts, denoted $\phi_{\text{opt-elec}}$, are independent of the identity of the neuron and the amplitude of the rhythmic neuronal response.

To determine whether the above conditions on $\phi_{\text{opt-elec}}$ were fulfilled, we measured the amplitude and phase of the optical signals as a function of the frequency of a rhythmic drive under voltage clamp for seven different types of neurons (45 neurons) A priori, we expected that measurements of amplitude would be influenced by variability between preparations, such as differential staining of neuronal versus nonneuronal tissue, while measurements of phase shift would be independent of these factors and thus have lower variance across measurements. We observed, for a drive of 5 mV in amplitude from an average holding potential of $-40$ mV, that the amplitude of the optical response decreased with increasing frequency over the range $0.2 \text{ Hz} \leq \upsilon \leq 3$ Hz (Figure 3B) and that the observed phase shift varied smoothly as a function of frequency (Figure 3C). The observed frequency dependence was best fit with a time constant of $\tau = 0.36 \pm 0.10$ s (solid lines, Figures 3B and

3C). This second estimate of $\tau$ is within the standard error of the value derived from the step response (Figure 3A).

Of critical importance for our studies, the observed phase at a fixed frequency was independent of the identity of the neuron analyzed (Figure 3C). Further, the shift was independent of the amplitude of the rhythmic potential (Figure 3D). These relationships show that the optical signal may be used to obtain accurate phase information for each active neuron. For the 1 Hz swim rhythm, we observed a shift of $\phi_{opt\text{-}elec} = 0.32\ \pi \pm 0.01\ \pi$ radians (mean $\pm$ SEM) (arrow, Figure 3C). This shift is a constant that may be subtracted from the phase of the measured coherence for all neurons in an optical field.

### Phase-Sensitive Detection

As a means of maximizing our ability to detect rhythmic signals with low signal-to-noise ratios, we characterized the involvement of each neuron in a rhythmic pattern in terms of the value of the coherence between the optical signal for the neuron and a common reference. The coherence is a complex valued function of frequency whose magnitude has a value of one for spectral components that covary with a constant phase shift and whose magnitude has a value that is less than one for components that fluctuate independently. In our analysis, neurons were considered to be phase locked to the reference signal when the magnitude of their coherence exceeded a threshold value, chosen as a 95% confidence level and calculated in two independent ways (see Experimental Procedures). The phase of the coherence, after subtraction of the common shift $\phi_{opt\text{-}elec}$, determines the timing of the rhythmic output relative to that of the reference. We denote the corrected phase shift as $\Delta\phi$, with the convention that positive values of $\Delta\phi$ correspond to a lag in phase relative to the reference.

### Imaging Neuronal Connectivity

To test the ability of our methodology to detect subthreshold potentials, we used phase-sensitive detection to delineate the postsynaptic followers of a driven neuron. We injected a sinusoidally varying current into an identified neuron and then calculated the coherences between the optical records of all of the neurons in the field and the intracellular potential of the driven neuron. The magnitude of the coherence indicated which neurons in the field followed at the drive frequency. The phase of the coherence determined the sign of the connection, i.e., $\Delta\phi \approx 0$ radians for excitatory connections and $\Delta\phi \approx \pi$ radians for inhibitory connections.

Our first test was to verify the monosynaptic inhibition between an identified dorsal inhibitor motor neuron, Cell 1, and a dorsal excitor, Cell 3 (Ort et al., 1974; Granzow et al., 1985). Cell 1 was driven by a sinusoidal current at 1 Hz. In agreement with the known connectivity, the intracellular potential in Cell 3 was nearly antiphasic ($\Delta\phi = 1.29\ \pi$ radians) with the intracellular potential of Cell 1 (cf. E1 and D3, Figure 4A). The corresponding optical signals from these cells exhibited strong peaks in their spectral power at 1 Hz (Figures 4B and 4C). The magnitude of the coherence between the respective optical records and the intracellular reference at 1 Hz was near a value of one and well above the 95% confidence level. Notably, a strong coherence was observed

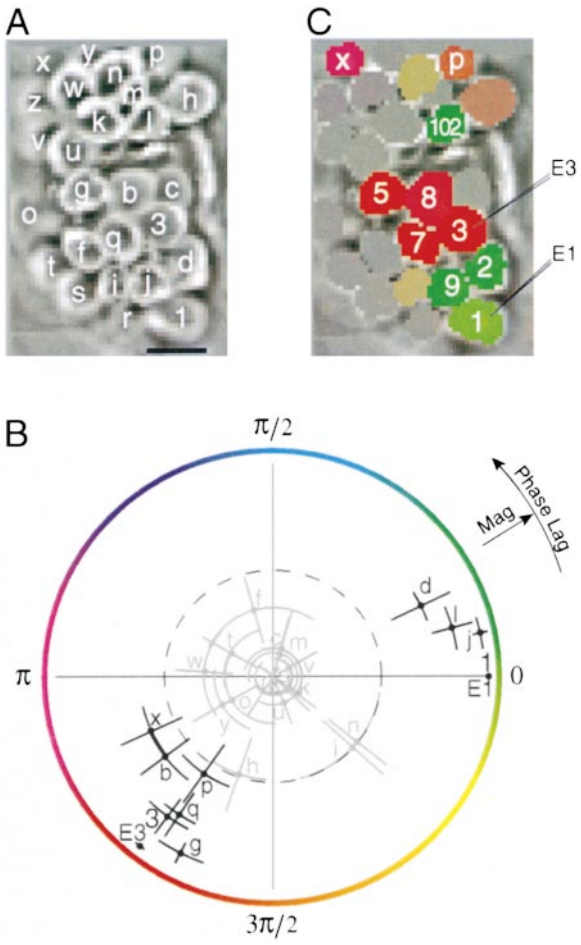


Figure 5. Optical Response of Dorsal Neurons to Sinusoidal Current Injected into Cell 1 (2 nA, 1 Hz)

All data are from the same 14 s trial used for Figure 4.

(A) Image of the optical field. Letters are assigned to each cell for analysis, with the exception of the impaled neurons, Cell 1 and Cell 3, which are indicated by numbers. The intracellular potential of Cell 1 serves as the phase reference for the coherence. Scale bar, 50 $\mu$m.

(B) Polar plot of the coherence for all neurons, relative to the phase of Cell 1, at the $\upsilon = 1$ Hz drive frequency. The letters correspond to the labeled neurons in (A). The bars indicate standard deviations. The absolute phase for all optical measurements was rotated by $\phi_{opt\text{-}elec} = 0.28\ \pi$ radians to place the phase of the optical signal for Cell 1 at 0 radians. The dashed circle indicates the 95% confidence level. Neurons for which the magnitude lies below the confidence level are depicted in gray.

(C) Optical field, with the location of each neuron coded according to coherence phase (color hue) and magnitude (color saturation) using the values and color code shown in (B). The color saturation was adjusted so that 18% gray corresponded to the 95% confidence level. The identification of neurons was based on anatomical location relative to Cell 1 and Cell 3; see Figure 6A for the canonical map of the dorsal aspect of leech segmental ganglia.

despite the relatively low signal-to-noise ratio of the optical signal for Cell 3 (Figure 4C). The phase difference between the measured coherence for the two cells was $\Delta\phi = 1.30\ \pi$ radians, consistent with the direct electrical measurement (Figure 4A). These results were seen in four preparations, for which $|\Delta\phi_{opt} - \Delta\phi_{elec}| = 0.09\ \pi \pm 0.10\ \pi$ radians (mean $\pm$ SD).

The connections from Cell 1 to other neurons in an

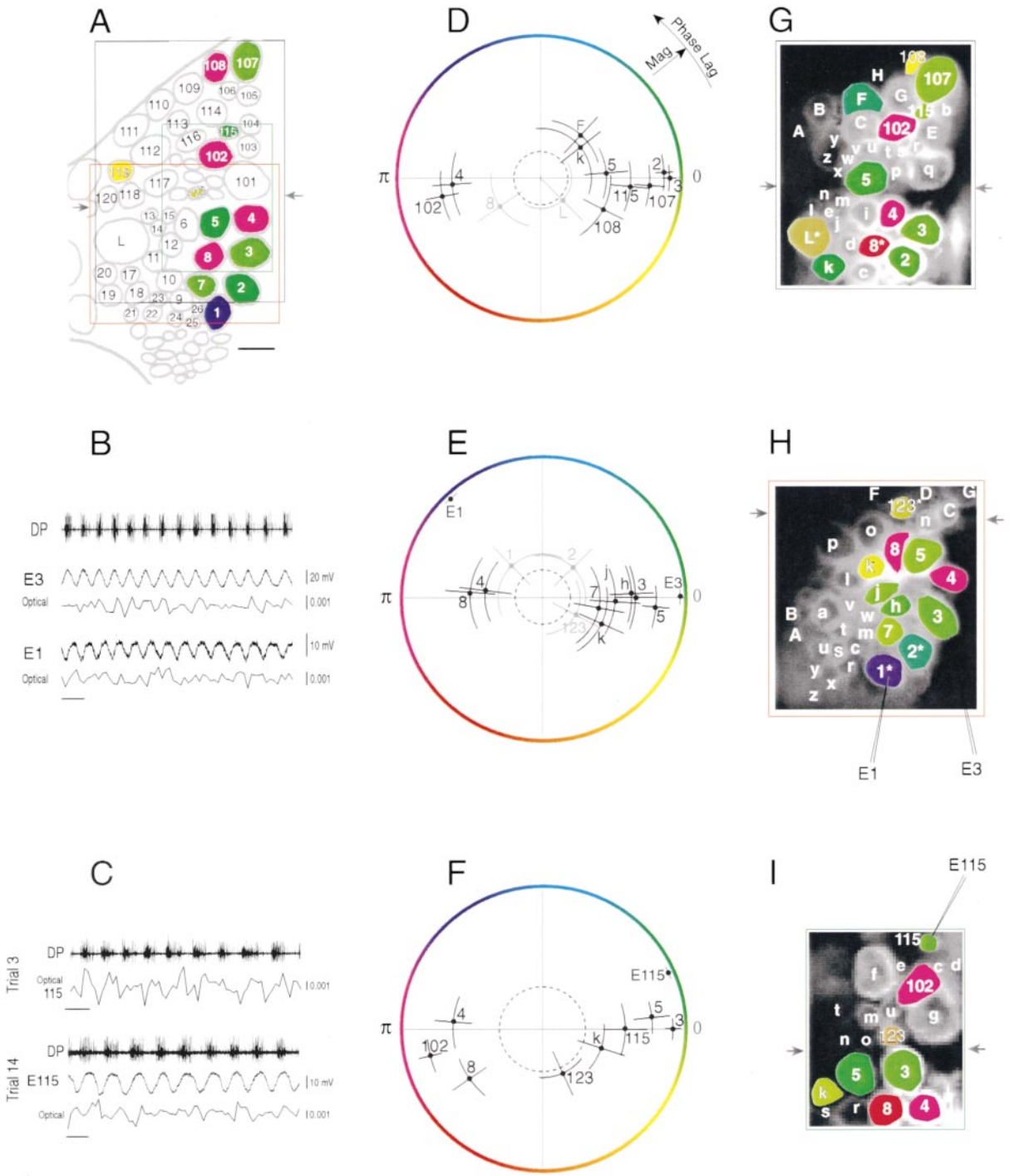


Figure 6. Optical Responses during the Generation of the Swimming Motor Pattern in an Isolated Nerve Cord

Shown are recordings from three different preparations in which all but the most posterior neurons on the dorsal surface of midbody ganglia were surveyed. Data from the three preparations are in separate rows: (D) and (G) (average of nine trials); (B), (E), and (H) (seven trials); and (C), (F), and (I) (three trials). Note that the absolute position of the somata varies between preparations and that in the images shown, the positions are sometimes distorted by the alignment and pitch of the ganglion and by changes in relative position produced by dissection.

(A) Map of identified neurons along the dorsal surface of the leech ganglion, shown in terms of the canonical scheme of Stent and coworkers (Muller et al., 1981). Neurons that have previously been identified as active in fictive swimming are shown in color, where the hue codes the phase (Brodfuehrer et al., 1995), as in (D) through (F). Note that the location of neurons on the map is approximate. Scale bar, 50 μm.

(B and C) Record of the spiking output from the DP nerve of the ganglion adjacent to the one being imaged, used to derive the reference signal, and simultaneous intracellular records and individual optical records during a swimming bout. In (B) are simultaneous recordings from a DP nerve, Cell 1, and Cell 3 on the fourth trial. In (C) are recordings from the DP nerve and Cell 115 before (trial 3) and after (trial 14) Cell 115 was impaled. Scale bars for optical traces indicate ΔF/F.

(D–F) Polar plots of the coherence for each neuron in the optical field (adjacent panels [G] through [I]). All diagrams are rotated so that the

optical field that encompassed the dorsal aspect of the ganglion (Figure 5A) were estimated by applying the above analysis to all cells in the field. We observed that eight neurons, in addition to Cell 3, showed significant coherent activation (Figure 5B); the phases of those neurons that exhibited significant coherence are shown as saturated color inserts in Figure 5C. The phases of the rhythmic activity of these neurons could be grouped into two clusters, one in synchrony with the output of Cell 1 ($\Delta\phi \approx 0.1\ \pi$ radians) and the other with a phase lag of $\Delta\phi \approx 1.3\ \pi$ radians (Figure 5B). The neurons that were synchronous with Cell 1 nominally occupied the location of a ventral inhibitor, Cell 2 (d in Figure 5A), a general inhibitor, Cell 9 (j), and a dorsal inhibitor, Cell 102 (l), all of which are known to be electrically coupled to Cell 1 (Ort et al., 1974). Four of the six neurons that oscillated out of phase with Cell 1 occupied the approximate location of dorsal excitors Cell 3, Cell 5 (g), and Cell 7 (q) and a ventral excitor, Cell 8 (b); these neurons are known to be synaptically inhibited by Cell 1 (Ort et al., 1974). The two additional neurons that oscillated out of phase with Cell 1 (x and p in Figures 5A and 5B) represent previously unknown followers of Cell 1 (confirmed in 10 of 13 trials).

### Imaging Neurons that Are Rhythmically Active in Fictive Swimming

To characterize the activity of neurons during fictive swimming, we focused on the dorsal hemiganglion and imaged overlapping optical fields that tiled much of this face of the ganglion (ten preparations). These fields encompassed many neurons that were previously shown to be involved in the swim rhythm (Figure 6A). An intracellular recording from Cell 3 or, equivalently, the spike pattern in extracellular recordings from the dorsal posterior (DP) nerve in an adjacent ganglion, whose output contains bursts of large spikes from Cell 3 during swimming cycles (Ort et al., 1974), served as the reference signal. The identity of neurons that were phase locked to the reference signal were inferred from their location and the phase of the coherence, and, for some preparations, the identification was confirmed by simultaneous intracellular recordings from selected neurons.

We consider neurons in a set of three fields that covered the anterior and much of the posterior dorsal hemiganglion (Figure 6). We calculated the coherence between the optical signals for each neuron in the optical field and the reference signal over multiple trials (three to nine), each of which was 10 s in duration. Many neurons in each field exhibited significant levels of coherence with the swim rhythm (Figures 6D–6I). Neurons in similar regions from different animals showed relatively consistent values for the magnitude and phase of the coherence (cf. Cells 3, 4, 5, and 8 in Figures 6G–6I).

We identified candidates for nearly all motor neurons that were previously determined to be active during swimming (Ort et al., 1974). The relative phase of their activity clustered into two groups, one synchronous with the output from Cell 3 (Cells 2, 3, 5, 7, and 107) and one with a phase lag near $\Delta\phi \approx \pi$ radians (Cells 1, 4, 8, and 102). Notably, the phase shift between Cells 1 and 3 during swimming was the same as that observed when Cell 1 was driven directly (cf. Figures 5B and 6E). We also observed significant rhythmic activity in presumptive motor neurons that have not previously been related to swim activity. In the posterior regions, which encompass excitors of longitudinal and circular muscle (Muller et al., 1981), several large neurons in the vicinity of Cells 9–15 were seen to have activity in phase with Cell 3 (k in Figures 6D and 6G and in Figures 6F and 6I, and h, j, and k in Figures 6E and 6H). In the anterior region, a large neuron in the neighborhood of Cell 110 was active, with a phase shift of $\Delta\phi \approx 0.3\ \pi$ radians (F in Figures 6D and 6G).

Our statistical criterion that the magnitude of the coherence exceed two independent estimates of the 95% confidence limit appeared to be conservative. Two examples are considered. In the first, the magnitude of the coherence was significant for only one of the two confidence estimates for a set of trials that involved Cell 1 (Figure 6B). However, the relative phase shift determined from the optical records was confirmed by impaling this cell and recording the intracellular potential of Cell 1 relative to that of Cell 3 (Figure 6E). In a second example, the output of the L Cell was observed to vary approximately in phase with that of Cell 3 (Figures 6D and 6G). The L Cell is known to receive rhythmic hyperpolarization during swimming (Ort et al., 1974).

The online computation of the coherence allowed us to impale and confirm the identity of interneurons. The somata of these neurons are generally small compared with those of motor neurons, with concomitantly less emission and a lower signal-to-noise ratio for their detection. We were thus concerned that interneurons might not be identified accurately. In one field (Figure 6I), the online computation revealed a small cell near the anterior midline with significant coherence (trial 3, Figure 6C). The rhythmic output of this neuron was nearly synchronous with that of Cell 3 (Figure 6F). Intracellular recording from this cell (trial 14, Figure 6C) confirmed that it produced an oscillating potential with the known phase relation and amplitude for Cell 115 (Brodfuehrer et al., 1995). This neuron was identified in four

phase of Cell 3 in each preparation is aligned at $\Delta\phi = 0$ radians because the bursts in the DP recording, used to define the reference phase, are produced during the peak depolarization of Cell 3 (Ort et al., 1974). Dashed circles represent the 95% confidence level, computed from randomized data sets (see Experimental Procedures), for the magnitude. Data for neurons whose coherence was not significant by two criteria are not shown, with the exception of specific cases (see text) depicted in gray. The labels E1, E3, and E115 refer to intracellular recordings from the respective neurons. For (F) only, in which the activity of Cell 3 was determined from the activity of the DP nerve in a neighboring ganglion, the interganglionic phase shift of 0.08 $\pi$ radians (Kristan et al., 1974) was subtracted.

(G–I) High-resolution images of the optical fields for each session. The approximate overlap of the fields with the map of the dorsal aspect of the ganglion is indicated by the frames in (A). The gray arrows mark the boundary between anterior and posterior packets. The pixels assigned to each cell are color coded according to the value of the phase of the coherence; neurons for which the magnitude of the coherence was not significant are not coded, with the exception of specific cases (asterisk). The numbers assigned to different neurons refer to the canonical scheme in (A).

preparations (Figures 6D and 6G), as was a second interneuron, Cell 123 (Figures 6E and 6H, and 6F and 6I), which is otherwise difficult to detect (P. D. B., unpublished data).

## Discussion

We have used optical imaging to survey the output of many neurons in a ganglion and to discriminate those that participate in a rhythmic motor activity. Our methods relied on FRET-based potentiometric indicator systems (Figure 1A), which previously had been shown to work on cultured cells. The present work now shows that such dye pairs can be useful and advantageous with neurons in intact assemblies.

The improved voltage sensitivity of the FRET pairs compared with past indicators (Figure 2C), together with estimates of phase coherence that minimize spectral variance (Figure 4), was applied to assay candidate neurons on the dorsal surface of leech ganglia that participate in fictive swimming (Figure 6). We discriminated 12 of the 13 neurons from optical fields of $\sim$50 neurons that were, based on intracellular recording, reported to be active in swimming (Brodfuehrer et al., 1995). We further correctly identified the phase of the output of these neurons in the swim cycle. In addition, we found novel cells that may participate in swimming (Figure 6). The specific role of these neurons in the generation of the swim rhythm will be a matter of additional investigation.

### The Coumarin Donor CC3

The third generation coumarin donor CC3 (Figure 1B) was designed to have only one long alkyl chain and to be a zwitterion at physiological values of pH. The previous coumarin-labeled phosphatidylethanolamine, CC1 (Figure 1B), had two alkyl chains and a net charge of $-2e$. An adsorbed CC3 coumarin should contribute about half as much additional cross-sectional area to the outer leaflet of the plasma membrane as a CC1 molecule would. Further, there should be little net electrostatic interaction between CC3 zwitterions and oxonols, whereas CC1 dianions could repel the oxonol, contrary to the goal of efficient FRET from coumarins to oxonols on the same leaflet of the membrane. We observed that CC3 indeed performed better than CC1, but most importantly, CC3 had less deleterious effect on cell input resistance (Figure 1E). This advantage might be explainable from the design features of CC3. The adsorption of dianionic CC1 to the outer leaflet of the membrane is expected to decrease the electric field across the membrane, which mimics depolarization, whereas zwitterionic CC3 would avoid this effect.

### Frequency-Domain Analysis

Phase-sensitive detection of rhythmic optical changes is a form of temporal averaging that is appropriate for the study of neural systems with periodic electrical activity. This naturally includes CPGs, in which a measure of motor output provides a coherence reference signal. Phase-sensitive detection should also be appropriate for sensory systems that are driven by periodic inputs, such as the auditory system or the electroreceptor system in fish. In the absence of an external reference, one can examine the spectral coherence between optical signals as a function of spatial location (Mann and Park, 1994), as has been done to detect periodic electrical waves among populations of neurons in a visual cortex (Prechtl et al., 1997) and an olfactory nucleus (Mitra and Pesaran, 1998). Finally, phase-sensitive detection provides a means of detecting spatially extended features of a driven neuron (Borst et al., 1997), as well as the postsynaptic follower cells of a driven neuron (Figure 5).

Here, the magnitude of the coherence was used as a means of testing for statistically significant phase-locked oscillatory activity relative to a value set by the level of noise. This interpretation will need to be revised under conditions of high signal-to-noise ratio. In this limit, the coherence may be significant, yet the actual change in voltage may be too small for the neuron to effectively contribute to the rhythm. Further, a neuron may be hyperpolarized and thus not contribute to swimming, as in the case of the L Cell (Figure 6) (Ort et al., 1974), yet still have a rhythmic component. On the other hand, the strict criteria adopted in the past, in which electrical stimulation of "pattern generating" cells must perturb the rhythm (Stent et al., 1978), are sufficient but not necessary criteria since the redundant nature of distributed networks allows them to function in the absence of specific neurons.

### Improvements

With the present equipment and levels of optical excitation, we could detect neurons with voltage swings as low as 2 mV (peak to peak) over the period of a swim bout, about ten cycles, close to the noise limitation. However, technical noise sources, such as motion of the preparation and wander of the arc in the illuminator, often decreased this sensitivity to swings of 5 mV over a swim bout. The dominant contribution to the shot noise was emission from dye that was outside of neuronal membrane. Optical sectioning, either by spatial modulation of the illumination (Neil et al., 1997) or by a scanning technique (Pawley, 1995), will reduce contributions from inactive tissue and from out-of-focus light and will increase the sensitivity of future measurements. Replacement of the coumarin donor by a genetically targetable fluorophore might help confine the optical signal to specific cells. Reduction of technical noise sources and an increase in signal can be achieved by simultaneously measuring the emission from both the oxonol and the coumarin molecules (Gonzalez and Tsien, 1995).

Oxonols with faster equilibration times across the membrane will be required in order to study CPGs or other circuits with dynamics faster than $\sim$1 Hz. Faster dyes are more hydrophobic, however, and are thus harder to load into tissue. We used an ethyl oxonol because of the ease and uniformity of staining and the high sensitivity to the transmembrane potential ($\beta = 0.8$ [Figure 2C] versus 0.4 for a "fast" oxonol [Gonzalez and Tsien, 1995]), even though signals were diminished by 2- to 3-fold at the swim frequency (Figure 2C). It is encouraging that preliminary attempts to load a butyl oxonol, with a time constant of $\tau = 20$ ms in cell culture

(Gonzalez and Tsien, 1997), have been successful and have yielded optical signals.

### Experimental Procedures

#### Preparation

Our subjects were adult *Hirudo medicinalis* (~3 g in mass) that were obtained from Leeches USA and maintained in 15°C artificial pond water. The dissection procedure has been described (Ort et al., 1974). Preparations that were used for assays consisted of single, midbody ganglia, while those used for fictive swimming consisted of the second through twenty-first midbody ganglia plus the tail brain. We typically desheathed the dorsal surface of the twelfth ganglion and stained and imaged this segment. Motion artifacts were minimized by pinning small pieces of sausage casing across the connectives immediately adjacent to the ganglion. Leech Ringer solution consisted of 115 mM NaCl, 4 mM KCl, 1.8 mM $CaCl_2$, 1.5 mM $MgCl_2$, 10 mM glucose, and 10 mM Tris-(hydroxymethyl)aminomethane buffer (pH 7.4).

#### Coumarin Synthesis

The precursor N-(2−dimethylaminoethyl)-6-chloro-7-(benzyloxymethoxy) coumarin-3-carboxamide was synthesized as follows (Equation 1). A mass of 241 mg of 3−carboxy−6−chloro−7−hydroxycoumarin (1 mmol) was dissolved in a mixture of 5 ml tetrahydrofuran (THF) and 5 ml dimethylformamide. A volume of 0.2 ml (1.2 mmol) of N,N-diisopropylethylamine (DIEA) and 330 mg (1.1 mmol) of O-(N-succinimidyl)-N,N,N',N'−tetramethyluronium tetrafluoroborate (TSTU) were added to the reaction mixture, which then was stirred at room temperature for 20 min under a nitrogen atmosphere. A 0.4 ml volume of DIEA and a 0.46 ml volume of benzyl chloromethyl ether were further added, and the mixture was stirred for an additional 2 hr. The solvents were next removed from the reaction mixture under high vacuum for 2 hr, and then a volume of 0.48 ml (4.4 mmol) of N,N-dimethylethylenediamine in 1 ml of THF was added. After 1 hr of further reaction, the solvents were again removed under high vacuum. The crude residue was purified by chromatography on silica gel and eluted with 5% methanol in chloroform to give a colorless solid with a mass of 190 mg (44% yield). $^1$H nuclear magnetic resonance on the final product, dissolved in $CDCl_3$, yielded chemical shifts of (in ppm): 2.32 (d, 6H), 2.56 (t, 2H), 2.16 (t, 2H), 4.76 (s, 2H), 5.46 (s, 2H), 7.33 (m, 7H), 7.68 (s, 1H), and 8.76 (s, 1H). Positive ion mass spectroscopy of the product, $C_{22}H_{23}O_5N_2Cl + H^+$, yielded a molecular weight of 431.2 g/M versus a calculated weight of 431.3 g/M.

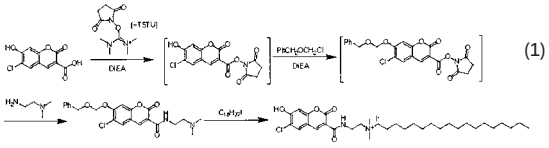


(1)

The iodide salt of the dye CC3 was prepared as follows (Equation 1). A mass of 43 mg (0.1 mmol) of the above product was dissolved in dichloromethane, to which 43 mg of 1-iodooctadecane (0.113 mmol) was added, and the mixture was heated to 80°C and stirred for 24 hr under a nitrogen atmosphere. After evaporation under high vacuum, the crude product was purified by chromatography on silica gel and eluted with 20% (v/v) methanol in chloroform to give a yellow solid product with a mass of 30 mg (53% yield). $^1$H nuclear magnetic resonance on the final product, dissolved in $CD_3OD$, yielded chemical shifts of (in ppm): 0.90 (t, 3H), 1.28 (m, 35H), 3.17 (s, 6H), 3.56 (t, 2H), 3.90 (t, 2H), 6.73 (s, 1H), 7.78 (s, 1H), and 8.69 (s, 1H). Positive ion mass spectroscopy of the product, $(C_{32}H_{52}ClN_2O_4)^+ + I^-$, yielded a molecular weight of 563.4 g/M versus a calculated weight of 563.5 g/M.

#### Coumarin Staining

We prepared a solution of 100 μM coumarin (CC3) in leech Ringer with 0.1% (w/v) pluronic F-127 (P-6867, Molecular Probes). Preparations of single ganglia were placed in a 2.0 ml microcentrifuge tube (05–408–25, Fisher Scientific) that contained 250 μl of dye solution and were agitated on a shaking table for 30 min. Whole nerve cord preparations, used for swim preparations, were first pinned out in a dish filled with Sylgard, and the twelfth ganglion was isolated within a 500 μl chamber with a Vaseline seal. A 250 μl recirculated volume of coumarin solution was then continuously pumped directly onto the ganglion for 30 min. After staining, the preparation was rinsed in Ringer solution and transferred to the recording chamber.

#### Oxonol Staining

A bath solution that contained 8 μM bis(1,3-diethylthiobarbiturate)-trimethine oxonol (Tsien, 1976) (available as B-413, Molecular Probes) was applied at least 15 min before the onset of recording. The oxonol was allowed to remain in the bath during the course of the measurements. This did not hinder optical recordings, presumably because the oxonol rapidly equilibrates between membrane and aqueous phases, and the oxonol did not increase the background fluorescence since its absorption occurs largely outside the bandwidth of the excitation light and since it has a 20-fold less fluorescent yield in aqueous solution than in the membrane (Rink et al., 1980). Oxonol loading was accompanied by an increase in oxonol fluorescence and a quenching of coumarin fluorescence.

#### Voltage Dependence of Oxonol Emission

The sensitivity of the two-component FRET system to changes in transmembrane potential has a simple form when the fluorescent emission is proportional to the concentration of oxonol that is present in the outer leaflet of the membrane. In this case, $F \propto [O]_{outside} = \{1 + \exp(\beta eV/kT)\}^{-1}$. We further note that, in the present work, the nonspecific emission greatly exceeds that from functionally active membranes. Thus, the measured signal, denoted F, may be expanded as $F(V) \cong F_0 + (\partial F/\partial V)\Delta V$, where $F_0$ is the nonspecific emission and is taken as a constant. The sensitivity of the emission to changes in neuronal transmembrane potential is

$$\frac{\Delta F}{F} \cong \frac{1}{F_0}\frac{\partial F}{\partial V}\Delta V = -A\left(\frac{2}{e^{\beta eV/2kT} + e^{-\beta eV/2kT}}\right)^2\left(\frac{\Delta V}{2kT/\beta e}\right), \qquad (2)$$

where A is a constant for a fixed drive frequency, and the minus sign indicates that a decrease in fluorescence corresponds to depolarization.

#### Di-4-ANEPPS Staining

The dye di-4-ANEPPS (Fluhler et al., 1985) (D-1199, Molecular Probes) was prepared at a concentration of 0.02% (w/v), as described (Delaney et al., 1994). Single ganglia were stained for a period of 1 hr, and then rinsed in leech Ringer solution.

#### Optical Recording

Measurements were made on an upright microscope configured for epifluorescence (UEM, Zeiss), using either 20× (0.5 NA, Olympus) or 40× (0.75 NA, Zeiss) water immersion objectives. Illumination was supplied by a 150 W xenon arc lamp (XBO, Osram) in a modified housing (66181, Oriel) that was powered by a constant current supply (1600, Optiquip). For the two-component FRET dye system, our filter system consisted of a 405 ± 15 nm (full width at half-maximum amplitude) band-pass excitation filter, a 430 nm dichroic mirror, a 460 ± 25 nm band-pass emission filter for the coumarin, and a 560 nm long-pass emission filter for the oxonol. The incident optical intensity was measured as required, with a small area photodiode placed in the focal plane, and was typically 20 mW/cm$^2$ with the 20× objective. At these light levels, the coumarin was bleached with a half-life of ~100 s. In the presence of oxonol, there was a small reduction in membrane resistance over the same 100 s period. For ganglia stained with di-4-ANEPPS, our filter system consisted of a 546 ± 5 nm band-pass excitation filter, a 580 nm dichroic mirror, and a 610 nm long-pass emission filter.

Images were acquired with a charge–coupled device camera (Photometrics PXL, EEV CCD-37 sensor) driven by IPLab Spectrum (Signal Analytics); the camera had a quantum efficiency of 10% at 450 nm (coumarin emission) and 25% at 550 nm (oxonol emission) and operated in the frame transfer mode. We recorded an image of the preparation at full resolution (up to 512 × 512 pixels) and recorded functional data from the same field at reduced spatial resolution (up to 85 × 85 pixels) at frame rates of 6–20 Hz. The outlines

of individual neurons were obtained from the full-resolution image and were used to label the signals from individual, reduced-resolution pixels that contributed to each of the neurons in the field. Unless noted, we recorded only the more sensitive emission from oxonol in the field of view.

The optical signal for each neuron was calculated as $\Delta F(t)/\bar{F} \equiv [F(t) - \bar{F}]/\bar{F}$, where F(t) is the spatially averaged fluorescence for the neuron in question and $\bar{F}$ is the time average of this fluorescence. A quartic polynomial was fit to the data and subtracted to remove the effects of bleaching (Figure 2A). All analysis, including spectral estimation (see below), was performed with programs that were written with Interactive Data Language (Research Systems).

### Electrophysiology

Intracellular recordings were made with 50–80 MΩ glass microelectrodes filled with 3 M K-acetate. All voltage-clamp measurements were made with two electrodes and a virtual ground (Axoclamp 2B, Axon Instruments). Intracellular signals, nerve signals, and camera synchronization pulses were acquired at a 1 kHz sampling rate and stored with programs that were written with LabVIEW (National Instruments). The electrical signals were averaged over the period of a camera pulse to form a common time base for use in spectral analysis.

### Fictive Swimming

Swimming was elicited by stimulating the DP nerve from a posterior ganglion with a 1 s long train of electrical pulses (1 V amplitude, 5 ms width, 10 Hz repetition) applied through a suction electrode. We recorded from the DP nerves in the eleventh or thirteenth ganglion as a reference signal. To facilitate swimming, 5-hydroxytryptamine (5-HT) was added to the Ringer solution for a final concentration of [5-HT] = 50 μM (Brodfuehrer et al., 1995).

Two physiological measures confirmed that isolated leech nerve cords produced normal swimming rhythms after staining with coumarin and oxonol. First, the spike pattern in extracellular recordings from the DP nerve was normal and produced bursts at the expected frequency of 1 Hz. Second, the phase difference between the output of motor neurons Cell 1 and Cell 3 during the swim rhythm, recorded with intracellular electrodes, was $\Delta\phi \approx 0.7\ \pi$ radians (Figure 6B); this is consistent with previous results (Granzow et al., 1985).

### Analysis

We used direct multitaper estimation techniques (Thomson, 1982) to calculate the power spectral densities, denoted $S_{opt}(\upsilon)$ and $S_{ref}(\upsilon)$ for the optical and reference signals, respectively, and their coherence, denoted $C(\upsilon)$. The use of multiple tapers provides a relatively balanced weight across all regions of a record, as opposed to the preferential weight given to the center of a record with only a single taper, and further, provides a means to estimate a standard deviation of the spectral estimates across a single trial. The spectral measures are defined by

$$S_{opt}(\nu) = \langle \tilde{V}_{opt}(\nu)\tilde{V}^*_{opt}(\nu)\rangle_{trials,\ tapers}, \tag{3}$$

with a similar expression for $S_{ref}(\upsilon)$, and

$$C(\nu) = \langle \tilde{V}_{opt}(\nu)\tilde{V}^*_{ref}(\nu)\rangle_{trials,tapers}/\sqrt{S_{opt}(\nu)S_{ref}(\nu)}. \tag{4}$$

The brackets denote an average over all trials and tapers, i.e., $\langle \tilde{V}(\nu)\tilde{U}(\nu)\rangle_{trials,tapers} \equiv (1/N)(1/K)\Sigma_{n=1}^{N}\Sigma_{k=1}^{K}\tilde{V}^{(n,k)}(\nu)\tilde{U}^{(n,k)}(\nu)$, where N is the number of trials, and K is the number of window functions or tapers, and $\tilde{V}^{(n,k)}(\nu)$ is the discrete Fourier transform of the product $w_k(t)V^{(n)}(t)$, i.e., the signal for the nth trial multiplied by the kth taper, $w_k(t)$. The sequences used to construct the tapers are an orthogonal set of functions (discrete prolate spheroidal sequences) (Slepian and Pollak, 1961; Percival and Walden, 1993) that minimizes the leakage of power between frequency bands.

The use of multiple tapers yields K independent estimates of the spectrum, which are averaged to form a final spectrum (Equations 3 and 4). The frequency resolution of the spectrum, defined in terms of half-width of the spectral bands, satisfies $\Delta\upsilon = (K + 1)/2T$ where T is the length of the data set. Estimates of spectral power were computed with K = 5 tapers, and estimates of coherence were computed with K = 11 tapers. For typical data sets (e.g., Figures 4B and 4C), T = 15 s, $\Delta\upsilon = 0.2$ Hz for spectral power, and $\Delta\upsilon = 0.4$ Hz for spectral coherence. Additional smoothing, but no change in bandwidth, is obtained by averaging the spectra from multiple trials.

Standard deviations of the coherence are reported as jackknife estimates within single trials (Thomson and Chave, 1991). In this procedure, the variance of a data set with K independent estimates of a quantity is found by deleting each estimate in turn and computing the variance over the K resulting averages. The "delete-one" averages of coherence, denoted $\hat{C}_j(\nu)$ where j is the index of the deleted taper, are given by

$$\hat{C}_j(\nu) = \langle \tilde{V}_{opt}(\nu)\tilde{V}^*_{ref}(\nu)\rangle_{trials,tapers\neq j}/\sqrt{S_{opt;j}(\nu)S_{ref;j}(\nu)}, \tag{5}$$

where $S_{opt;j}(\nu) = \langle V_{opt}(\nu)\tilde{V}^*_{opt}(\nu)\rangle_{trials,tapers\neq j}$, $S_{ref;j}(\nu)$ is similarly defined, and $\langle \ldots \rangle_{trials,tapers\neq j}$ denotes an average over all trials and all but one taper for a given trial, i.e., $\langle \tilde{V}(\nu)\tilde{U}(\nu)\rangle_{trials,tapers\neq j} = (1/N)[1/(K - 1)]\Sigma_{n=1}^{N}\Sigma_{k=1;\ k\neq j}^{K}\tilde{V}^{(n,k)}(\nu)\tilde{U}^{(n,k)}(\nu)$. We computed the standard deviation of the magnitude of $C(\upsilon)$ as

$$\sigma_{mag}(\nu) = \sqrt{[K - 1)/K]\Sigma_{j=1}^{K}|\hat{C}_j(\nu) - C(\nu)|^2} \tag{6}$$

The variance estimate for the phase of $C(\upsilon)$ is computed by comparing the relative directions of the delete-one unit vectors $\hat{C}_j(\nu)/|\hat{C}_j(\nu)|$. The standard deviation is computed as

$$\sigma_{\Delta\phi}(\nu) = \sqrt{2[(K - 1)/K](K - |\Sigma_{j=1}^{K}\hat{C}_j(\nu)/|\hat{C}_j(\nu)||} \tag{7}$$

Statistical confidence was established in two ways. An estimate of the 95% confidence interval was derived from a calculation of the probability distribution function for the coherence that was based on randomized data from all measured neurons and trials for a given preparation. We computed the distribution of the magnitudes of the coherence using shuffled optical signals (500 independently shuffled records for each trial) and the measured reference signal. We chose our confidence level as the 0.95 level of this distribution. A second estimate was defined as twice the standard deviation (95% level for a normal distribution) of the magnitude of the coherence as determined from a jackknife estimate over multiple estimators of the coherence ($2\sigma_{mag}$; Equation 6). Unless noted, we required that the magnitude of the coherence at a particular frequency exceed both measures.

### Acknowledgments

We thank R. Wessel for collaborating on early aspects of this work; P. P. Mitra, B. Pesaran, and A. L. Taylor for valuable discussions; and B. Friedman for comments on early versions of the manuscript. Aspects of the analysis were formulated as part of the National Institute of Mental Health–sponsored workshop "Analysis of Neural Data" at the Marine Biology Laboratories. This work was supported by National Institutes of Health training grant GM08107 (T. W. C.), National Institutes of Health Senior National Research Service Award NS10479–01 (P. D. B.), National Institutes of Health research grants MH43396 (W. B. K.) and NS27177 (R. Y. T.), the Howard Hughes Medical Institute (S. R. A., R. Y. T.), and start-up funds from the University of California (D. K.).

Received May 5, 1999; revised June 16, 1999.

### References

Borst, A., Heck, D., and Thomann, M. (1997). Voltage signals of individual Purkinje cell dendrites in rat cerebellar slices. Neurosci. Lett. *238*, 29–32.

Brodfuehrer, P.D., Debski, E.A., O'Gara, B.A., and Friesen, W.O. (1995). Neuronal control of leech swimming. J. Neurobiol. *27*, 403–418.

Calabrese, R.L., Nadim, F., and Olsen, O.H. (1995). Heartbeat control in the medicinal leech: a model system for understanding the origin, coordination, and modulation of rhythmic motor patterns. J. Neurobiol. *27*, 390–402.

Canepari, M., Campani, M., Spadavecchia, L., and Torre, V. (1996). CCD imaging of the electrical activity in the leech nervous system. Eur. Biophys J. *24*, 359–370.

Delaney, K.R., Gelperin, A., Fee, M.S., Flores, J.A., Gervais, R., Tank, D.W., and Kleinfeld, D. (1994). Waves and stimulus-modulated dynamics in an oscillating olfactory network. Proc. Natl. Acad. Sci. USA *91*, 669–673.

Delcomyn, F. (1980). Neural basis of rhythmic behavior in animals. Science *210*, 492–498.

Fluhler, E., Burnham, V.G., and Loew, L.M. (1985). Spectra, membrane binding, and potentiometric responses of new charge shift probes. Biochemistry *24*, 5749–5755.

Forster, T. (1948). Intramolecular energy migration and fluorescence, R.S. Knox, transl., Ann. Physics (Leipzig) *2*, 55–75.

Friesen, W.O., Poon, M., and Stent, G.S. (1976). An oscillatory neuronal circuit generating a locomotory rhythm. Proc. Natl. Acad. Sci. USA *73*, 3734–3738.

Fromherz, P., and Lambacher, A. (1991). Spectra of voltage-sensitive fluorescence of styryl-dye in neuron membrane. Biochim. Biophys. Acta *1068*, 149–156.

Getting, P.A. (1989). A network oscillator underlying swimming in *Tritiona*. In Neuronal and Cellular Oscillators, J.W. Jacklet, ed. (New York: Marcel Dekker), pp. 215–236.

Gonzalez, J.E., and Tsien, R.Y. (1995). Voltage sensing by fluorescence resonance energy transfer in single cells. Biophys. J. *69*, 1272–1280.

Gonzalez, J.E., and Tsien, R.Y. (1997). Improved indicators of cell membrane potential that use fluorescence resonance energy transfer. Chem. Biol. *4*, 269–277.

Granzow, B., Friesen, W.O., and Kristan, W.B., Jr. (1985). Physiological and morphological analysis of synaptic transmission between leech motor neurons. J. Neurosci. *5*, 2035–2050.

Grillner, S., Wallen, P., Brodin, L., and Lansner, A. (1991). Neuronal network generating locomotor behavior in lamprey: circuitry, transmitters, membrane properties, and simulation. Annu. Rev. Neurosci. *14*, 169–199.

Kleinfeld, D., and Sompolinsky, H. (1988). Associative neural network model for the generation of temporal patterns: theory and application to central pattern generators. Biophys. J. *54*, 1039–1051.

Kristan, W.B., Jr., Stent, G.S., and Ort, C.A. (1974). Neuronal control of swimming in the medicinal leech. III. Impulse patterns of motor neurons. J. Comp. Physiol. A *94*, 115–176.

Loew, L.M., Scully, S., Simpson, L., and Waggonner, A.S. (1979). Evidence for a charge-shift electrochromic mechanism in a probe for membrane potential. Nature *281*, 497–499.

Mann, M.E., and Park, J. (1994). Global-scale modes of surface temperature variability on interannual to centuries timescales. J. Geophys. Res. *99*, 25819–25833.

Marder, E., and Calabrese, R.L. (1996). Principles of rhythmic motor pattern generation. Physiol. Rev. *76*, 687–717.

Mitra, P.P., and Pesaran, B. (1998). Analysis of dynamic brain imaging data. Biophys. J. *76*, 691–708.

Muller, K.J., Nicholls, J.G., and Stent, G.S. (1981). Neurobiology of the Leech (Cold Spring Harbor, NY: Cold Spring Harbor Laboratory Press).

Neil, M.A.A., Juskaitis, R., and Wilson, T. (1997). Method of obtaining optical sectioning by using structured light in a conventional microscope. Optics Lett. *22*, 1905–1907.

Obaid, A.L., Koyano, T., Lindstrom, J., Sakai, T., and Salzberg, B.M. (1999). Spatiotemporal patterns of activity in an intact mammalian network with single-cell resolution: optical studies of nicotinic activity in an enteric plexus. J. Neurosci. *19*, 3073–3093.

Ort, C.A., Kristan, W.B., Jr., and Stent, G.S. (1974). Neuronal control of swimming of the medicinal leech. II. Identification and connections of motor neurons. J. Comp. Physiol. A *94*, 121–154.

Pawley, J.W. (1995). Handbook of Biological Confocal Microscopy, Second Edition (New York: Plenum Press).

Percival, D.B., and Walden, A.T. (1993). Spectral Analysis for Physical Applications: Multitaper and Conventional Univariate Techniques (Cambridge, UK: Cambridge University Press).

Prechtl, J.C., Cohen, L.B., Mitra, P.P., Pesaran, B., and Kleinfeld, D. (1997). Visual stimuli induce waves of electrical activity in turtle cortex. Proc. Natl. Acad. Sci. USA *94*, 7621–7626.

Rink, T.J., Montecucco, T.R., Hesketh, T.R., and Tsien, R.Y. (1980). Lymphocyte membrane potential assessed with fluorescent probes. Biochim. Biophys. Acta *595*, 15–30.

Salzberg, B.M., Grinvald, A., Cohen, L.B., Davila, H.V., and Ross, W.N. (1977). Optical recording of neuronal activity in an invertebrate central nervous system: simultaneous monitoring of several neurons. J. Neurophysiol. *40*, 1281–1291.

Satterlie, R.A. (1985). Reciprocal inhibition and postinhibitory rebound produces reverberation in a locomotor pattern generator. Science *229*, 402–404.

Selverston, A.I., and Moulins, M. (1987). The Crustacean Stomatogastric System (New York: Springer-Verlag).

Slepian, D., and Pollak, H.O. (1961). Prolate spheroidal wave functions. I. Fourier analysis and uncertainty. Bell System Tech. J. *40*, 43–64.

Stent, G.S., Kristan, W.B., Jr., Friesen, W.O., Ort, C.A., Poon, M., and Calabrese, R.L. (1978). Neuronal generation of the leech swimming movement. Science *200*, 1348–1357.

Thomson, D.J. (1982). Spectral estimation and harmonic analysis. Proc. IEEE *70*, 1055–1096.

Thomson, D.J., and Chave, A.D. (1991). Jackknifed error estimates for spectra, coherences, and transfer functions. In Advances in Spectrum Analysis and Array Processing, S. Shykin, ed. (Englewood Cliffs, NJ: Prentice Hall), pp. 58–113.

Tsien, R.Y. (1976). The design and use of organic chemical tools in cellular physiology. PhD thesis, Churchill College, Cambridge University, Cambridge, United Kingdom.

Weeks, J.C., and Kristan, W.B., Jr. (1978). Initiation, maintenance and modulation of swimming in the medicinal leech by the activity of a single neurone. J. Exp. Biol. *77*, 71–88.

Youngentob, S.L., Kent, P.F., Sheehe, P.R., Schwob, J.E., and Tzoumaka, E. (1995). Mucosal inherent activity patterns in the rat: evidence from voltage-sensitive dyes. J. Neurophysiol. *73*, 387–398.

Yuste, R., Tank, D.W., and Kleinfeld, D. (1997). Functional charcterization of the cortical microcircuit with voltage-sensitive dye imaging of neocortical slices. Cereb. Cortex *7*, 546–558.

Zecevic, D., Wu, J.-Y., Cohen, L.B., London, J.A., Hoop, H.-P., and Falk, C.X. (1989). Hundreds of neurons in the Aplysia abdominal ganglion are active during the gill-withdrawal reflex. J. Neurosci. *9*, 3681–3689.